Nonlinear optical studies of binary mixtures of hydrogen bonded liquids

Jung Y. Huang and M. H. Wu
Institute of Electro-Optical Engineering, Chiao Tung University, Hsinchu, Taiwan, Republic of China
(Received 14 March 1994)

We applied two nonlinear optical techniques for investigating CH_3OH-H_2O and CH_3CN-H_2O binary liquid mixtures. The measured third-harmonic susceptibility of CH_3OH-H_2O with varying methanol mole fraction sensitively reflects the microstructure of the liquids. The perturbed polar distribution of methanol molecules by interfacial water at the vapor-liquid interface of CH_3OH-H_2O was revealed with infrared-visible sum-frequency generation (IVSFG). For CH_3CN-H_2O our third-harmonic-generation result clearly indicates the existence of microheterogeneity in a mixture with a mole fraction of acetonitrile larger than 0.3. By comparing with an IVSFG study of CH_3CN-H_2O reported by Eisenthal *et al.* [J. Chem. Phys. **98**, 5099 (1993)], the observed critical acetonitrile concentration for the onset of phase separation in CH_3CN-H_2O appears to be larger than that at the liquid surface.

PACS number(s): 61.25.−f, 68.35.Ja, 42.65.Ky

I. INTRODUCTION

Hydrogen bonded liquids, such as water, methanol and acetonitrile, exhibit peculiar thermodynamic behaviors [1]. These liquids and their binary mixtures are important solvents which are relevant to many chemical and biochemical processes [2]. The microstructure of these liquids is a subject of interest by itself, but the implications of the findings for the behavior of the mixtures are also of greater interest. For examples, CH_3OH-H_2O and CH_3CN-H_2O are well known as important media ranging from materials synthesis, electrochemistry, to liquid chromatography. From the interest of fundamental research, the loss of entropy associated with generating a cage of water molecules around hydrophobic head groups [3] has frequently been cited as the principle driving mechanism responsible for the folding of protein. Unfortunately, our understanding of these liquid systems is rather poor owing to the lack of suitable techniques with which the molecular structure can be probed [4]. In the past, such microstructural information of liquids was typically deduced from the measurements of thermodynamic quantities.

Over the past several years a number of nonlinear optical (NLO) techniques have been developed for investigating the bulk and interfacial properties of various media [5,6]. These techniques are particularly suited for studying those systems whose thermodynamic equilibrium states are susceptible to external perturbations. Second-order NLO effects in the bulk of an isotropic medium vanish under the electric-dipole approximation. However, owing to the symmetry breaking at the boundary of centrosymmetric media, the second-order NLO effects can occur and have surface specificity. Infrared-visible sum-frequency generation (IVSFG) belongs to the second-order NLO processes [5]. This technique also possesses an excellent molecular selectivity. It is thus ideal for identifying surface species and yielding their orientational distributions. Third-harmonic generation (THG) is the simplest process among many third-order NLO effects. Hence, in the past, it has been widely applied for investigating the bulk properties of a variety of materials [6].

In this paper, we show that important microstructural information about the molecules in the bulk and at the liquid-vapor interface of CH_3OH-H_2O can be revealed by combining the unique features of IVSFG and THG. The usefulness of the techniques is further confirmed by applying THG to resolve the controversial result of microheterogeneity in the bulk of CH_3CN-H_2O. The microstructure of the interfacial acetonitrile at the surface of CH_3CN-H_2O has been recently investigated by Zhang, Gutow, Eisenthal, and Heinz using IVSFG technique [7]. According to their result, a surface phase separation can occur with the bulk acetonitrile mol fraction higher than 0.07. It is thus interesting to know whether such a phase separation also sets in the bulk of CH_3CN-H_2O at a similar critical concentration. By using NLO techniques, we examine the microstructure of these two binary liquid mixtures in detail.

This paper is organized as follows. First, the experimental procedures are briefly described in Sec. II. Theoretical background of IVSFG and THG is presented in Sec. III. We apply the theories developed to analyze the experimental results, and then offer the discussion in Sec. V. Finally, conclusions are drawn.

II. EXPERIMENT

A. Infrared-visible sum-frequency generation

The experimental setup of IVSFG has been described elsewhere [8]. In the present experiment, the laser system produced visible pulses at 0.532 μm and tunable infrared pulses around 3.5 μm, with energies at the sample of 0.5 mJ (diam 700 μm) and 0.1 mJ (diam 300 μm), respectively. Both had a pulse width of $\sim$20 ps and a repetition rate of 10 Hz. The two beams were overlapped at the liquid-vapor interface of the solution in a Teflon trough enclosed in a cell. A 7° angular separation between the

input beams (see Fig. 1) was used to permit the separation of the second-harmonic ($\lambda_{SH}=266$ nm) and the sum-frequency ($\lambda_{SF}\sim 460$ nm) signals. The absorption of the incident infrared beam in the liquid was kept well below 5% by making the beam path in the vapor less than 2 mm. The tunable infrared source was calibrated to 1.5 cm^{-1} with a polystyrene reference and all spectra were normalized to the SF signal from a y-cut crystalline quartz. All the measurements were performed at room temperature.

In the case of IVSFG, the effective surface sum-frequency susceptibility near vibrational resonances can be written as

$$\chi^{(2)}_{s,\text{eff}}(-\omega_s;\omega_{\text{vis}},\omega_{\text{ir}})=\chi_{\text{NR}}+\sum_q \frac{A_q}{(\omega_{\text{ir}}-\omega_q+i\gamma_q)} , \quad (1)$$

where A_q, ω_q, and γ_q are the strength, resonant frequency, and damping constant of the qth mode, respectively. The resonant enhancement of $\chi^{(2)}_{s,\text{eff}}$ as ω_{ir} scans over ω_q then yields the surface-vibrational spectrum observed by IVSFG. The peak positions, strengths, and widths of a resonance can be determined by a fit of the SFG spectrum to the absolute square of Eq. (1) to remove the interfering effect among neighboring peaks and nonresonant background (χ_{NR}).

B. Third-harmonic generation

The experimental arrangement of THG measurements, detailed by Kajzar and Messier [9], is shown in Fig. 2. The excitation beam was from an injection seeded Q-switched Nd:YAG laser operating at 1.064 μm. The linewidth of the laser was narrower than 0.003 cm^{-1} with a transverse intensity distribution more than 90% close to the Gaussian profile. Hence the Gaussian distribution is adequate for depicting the temporal and spatial profiles of the laser during THG data analysis.

The pump beam was focused onto the liquid cell by a lens with a focal length of 40 cm. The confocal parameter ($b=2\pi n_1 w_0^2/\lambda_1$) of the resulting laser beam was found to be 9.98 mm, which corresponds to a radius of $w_0=34$ μm at the beam waist. The position of the liquid cell along the laser beam direction was carefully adjusted such that the beam waist was located at the center of the cell.

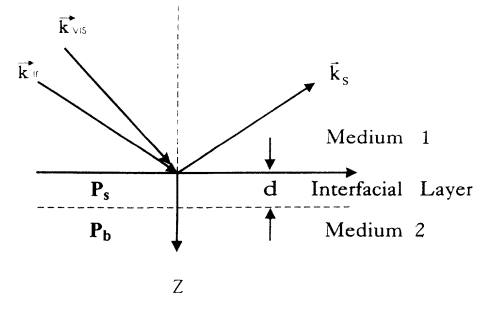

FIG. 1. Geometry of sum-frequency generation ($k_{\text{ir}}+k_{\text{vis}}\rightarrow k_s$) from an interface in the reflected direction. The polarization sheet (P_s) is embedded in a thin layer with a thickness d. The Z direction is taken as zero at the interface between the media and is positive going into medium 2.

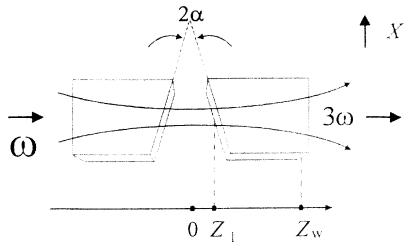

FIG. 2. Schematic diagram of a typical THG liquid cell. The wedge-shaped features on the left and right are the silica-glass windows. The liquid sample is inserted into the space between two wedge windows. The entire cell is translated in the X direction during THG measurements.

The liquids with spectroscopic grade were inserted between two fused silica windows with a wedge angle of $\alpha=0.7°$. Flatness of these windows is better than $\lambda/10$. All THG measurements of the binary liquid mixtures at different concentrations were performed under the same experimental condition. Third-harmonic-generation signals are calibrated to that from the silica glass window which is known to have a third-order susceptibility of 3.11×10^{-14} esu [9].

III. THEORETICAL CONSIDERATIONS

A. Infrared-visible sum-frequency generation from a liquid-vapor interface

A phenomenological treatment of the nonlinear optical response of an interface has been reported [10]. It bases upon the notion that on the microscopic scale, both the optical field and the dielectric constant cannot vary abruptly across the interfacial layer. With Z normal to the interface, we assume that the dielectric constant of the interface $\varepsilon(Z)$ varies from ε_1 to ε_2 along Z across the interface (see Fig. 1). The field component parallel to the interface is always continuous, but the component along Z takes the form $E_z(Z)=D_z(Z)/\varepsilon(Z)$, with the displacement current component D_z being continuous across the interface. For media with an inversion symmetry such as vapor-liquid discussed here, the reflecting SF electric field in the medium 1 (vapor), radiated by the surface nonlinear polarization $\mathbf{P}_s$ (ω_s) and the bulk nonlinear polarization $\mathbf{P}_b$ (ω_s), can be effectively viewed to originate from an infinitesimally thin interfacial layer with the nonlinear response described by an effective surface NLO susceptibility $\chi^{(2)}_{s,\text{eff}}$. From this model, $\chi^{(2)}_{s,\text{eff}}$ can be grouped into three distinctive terms [11]:

$$[\chi^{(2)}_{s,\text{eff}}]_{ijk}=\chi^{(2)}_{D,ijk}+[\chi^{(2)}_{B,ijk}+\chi^{(2)}_{I,ijk}]$$
$$=\chi^{(2)}_{D,ijk}+[\chi^{(2)}_{Q,ijk}] . \quad (2)$$

Here, $\chi^{(2)}_Q$ is electric quadrupole in nature (i.e., originating from the nonlocal response of the interface). It consists of two parts. The first part $\chi^{(2)}_B$ has the origin in the structural disparity leading to different quadrupole

responses in media 1 and 2; while the second term $\chi_I^{(2)}$ comes from quadrupole response from the rapid variation of the incoming field across the interface. $\chi_D^{(2)}$ arises from the electric-dipole contribution (i.e., the local response) of the surface layer. Because of the broken inversion symmetry at the interface, this term is nonvanishing even if the bulk is centrosymmetric.

Formally, we can express the sum-frequency (SF) susceptibility in terms of the corresponding nonlinear molecular polarizability as [5,11]

$$\chi^{(2)}_{D,ijk}=N_s \sum_{I,J,K} \langle (Ii)(Jj)(Kk)\rangle \alpha^{(2)}_{D,IJK} , \tag{3}$$

where $N_s=Nd$ is the surface density of molecules, and $\langle\ \rangle$ denotes the orientational average. For a binary liquid mixture of A-B at a mole fraction of c_A, the effective surface SF susceptibility at the qth normal mode of molecule A, normalized with that of the neat liquid, can be expressed as

$$\bar{\chi}^{(2)}_{s,\text{eff}}(c_A)=\frac{\chi^{(2)}_{s,\text{eff}}(c_A)}{\chi^{(2)}_{s,\text{eff}}(c_A=1)}=\frac{\bar{N}_s(c_A)G_A(c_A)\chi^{(2)}_D+c_A\chi^{(2)}_Q}{\chi^{(2)}_D+\chi^{(2)}_Q}$$
$$=\frac{\bar{N}_s(c_A)G_A(c_A)\bar{\chi}^{(2)}_D+c_A}{\bar{\chi}^{(2)}_D+1} , \tag{4}$$

where $\bar{\chi}^{(2)}_D=\chi^{(2)}_D/\chi^{(2)}_Q$; $\bar{N}_s(c_A)=N_s(c_A)/N_s$ $(c_A=1)$ is the normalized surface density of species A at the surface of the liquid mixture; $G_A(c_A)$ denotes the enhancement of the polar order at the vapor-liquid interface of the mixture compared with that of neat liquid. Here the bulk contribution $\chi^{(2)}_Q(c_A)$ from species A is proportional to its mole fraction. We can deduce $G_A(c_A)$ and $\bar{\chi}^{(2)}_D$ from the fit of the measured $\chi^{(2)}_{s,\text{eff}}(c_A)$ to Eq. (4) with the known $\bar{N}_s(c_A)$.

B. Third-harmonic generation from a liquid

Third-harmonic conversion with focused Gaussian beams has been discussed by Ward and New [12] and by Puell *et al.* [13]. Bjorklund [14] has given an extensive discussion of four-wave sum- and difference-frequency mixing with focused beams. In this section, we shall briefly discuss third-harmonic generation of a focused Gaussian beam which will be used in data analysis.

Assuming the electric field of the focused pump beam has the form

$$E_1(r,z)=\tfrac{1}{2}\{A_1(r,z)e^{ik_1z-i\omega_1t}+\text{c.c.}\} ,$$
$$A_1(r,z)=\frac{A_{10}}{(1+i\xi)}\exp\left[-\frac{k_1r^2}{b(1+i\xi)}\right] , \tag{5}$$

where $b=k_0n_1w_0^2$ is the confocal parameter of the pump beam; w_0 is the radius at the $1/e$ of the field profile; and $\xi=2(z-z_0)/b$ denotes the distance to the beam waist (z_0) normalized by the Rayleigh range $(b/2)$. In media with a third-order nonlinearity, the pump beam can induce nonlinear polarization which then serves as the radiation source of the third-harmonic (TH) field. Under the assumption of nondepleted pump beam and slowly varying amplitude approximation, the coupled-wave equations that govern the pump and TH field amplitudes are simplified to the following equation

$$\nabla_1^2A_3+2ik_3\frac{\partial A_3}{\partial z}=-\frac{\pi\omega_3^2}{c^2}\chi^{(3)}A_1^3e^{-i\Delta kz} , \tag{6}$$

where $\Delta k=k_3-3k_1=6\pi[n_3(\omega_3)-n_1(\omega_1)]/\lambda_1$ denotes the phase mismatch of the frequency conversion. In general, Δk is much smaller than k_3 and k_1. If the confocal parameter and the beam waist location of the TH field are the same as that of the pump beam, the TH field amplitude $A_3(r,z)$ radiated from the material extending from z' to z can be readily obtained with Eq. (6),

$$A_3(r,z)=i\frac{3\pi^2b}{2n_3\lambda_1}\chi^{(3)}\frac{A_{10}^3}{[1+i\xi(z)]}\exp\left\{-\frac{3k_1r^2}{b[1+i\xi(z)]}\right\}$$
$$\times e^{-i\Delta kz_0}\int_{\xi(z')}^{\xi(z)}\frac{e^{-ib\Delta k\xi''/2}}{(1+i\xi'')^2}d\xi'' . \tag{7}$$

If $b\Delta k\gg1$, the integral in Eq. (7) is effectively contributed from two slabs [12], each has a thickness of one coherent length and positions at one of the integration limits. The total TH amplitude on the far right side of the liquid cell (see Fig. 2) is the summation of the TH fields generated by air, wedge windows, and liquid. If the beam waist and the center of the liquid cell are properly overlapped at $z_0=0$, we then have the total TH amplitude as

$$E_3(r,z)\propto\frac{T_1+AT_0}{1+\xi^2(-z_w)}e^{i[-2\tan^{-1}\xi(-z_w)+6k_0z_l(N_L-N_G)]}+\left[\frac{T_1}{1+\xi^2(-z_l)}+\frac{T_2R}{1+\xi^2(-z_l)}\right]$$
$$\times e^{i[-2\tan^{-1}\xi(-z_l)+3k_0z_l(2N_L-n_G-N_G)]}+\left[\frac{T_3}{1+\xi^2(z_l)}+\frac{T_2R}{1+\xi^2(-z_l)}\right]$$
$$\times e^{i[-2\tan^{-1}\xi(z_l)+3k_0z_l(2n_L-n_G-N_G)]}+\frac{T_3+AT_4}{1+\xi^2(z_w)}e^{i[-2\tan^{-1}\xi(z_w)+6k_0z_l(n_L-n_G)]} , \tag{8}$$

where $N_i\equiv n_i(3\omega)$ and $n_i\equiv n_i(\omega)$ represent the index of refraction of the medium i at the frequency of 3ω and ω; $A\equiv(\chi^{(3)}/\Delta\varepsilon)_{\text{air}}/(\chi^{(3)}/\Delta\varepsilon)_{\text{glass}}$ and $R\equiv(\chi^{(3)}/\Delta\varepsilon)_L/(\chi^{(3)}/\Delta\varepsilon)_{\text{glass}}$ are the TH susceptibility of air and liquid normalized with that of the glass window. By referring to the cell geometry depicted in Fig. 2, we note that the first and fourth terms of Eq. (8) are contributed from air and glass at the two air-glass interfaces; while the second and the third terms can be attributed to the joint contributions of liquid and glass at the glass-liquid interfaces. Here T_i $(i=0\sim4)$ denote the effective transmission coefficient for each field, and they are found to have the following expressions:

$$T_0=T_{AG}T_{GL}T_{LG}T_{GA};\quad T_1=t_{AG}^3T_{GL}T_{LG}T_{GA};\quad T_2=(t_{AG}t_{GL})^3T_{LG}T_{GA};$$
$$T_3=(t_{AG}t_{GL}t_{LG})^3T_{GA};\quad T_4=(t_{AG}t_{GL}t_{LG}t_{GA})^3\ . \tag{9}$$

T_{ij} (and t_{ij}) indicates the Fresnel transmission factor of the TH (and the pump) field as it propagates from medium i to j. By examining Eq. (8), we find that T_0 and T_4 are the effective transmission coefficients for the TH fields generated from air outside the entrance and exit glass windows. In addition, the TH field originating from the entrance (and exit) glass window has an effective transmission coefficient of T_1 (and T_3). Finally, the transmission factor for the TH field from the liquid is T_2.

By taking the absolute square of Eq. (8), the total TH intensity from the liquid cell can be expressed as

$$\begin{aligned}I(3\omega)=&I_1+I_2\cos[2\tan^{-1}\xi(-z_l)-2\tan^{-1}\xi(-z_w)-3k_0z_l\Delta n_G]\\&+I_3\cos[2\tan^{-1}\xi(z_l)-2\tan^{-1}\xi(-z_w)-3k_0z_l(\Delta n_G-2\Delta n_L)]\\&+I_4\cos[2\tan^{-1}\xi(z_w)-2\tan^{-1}\xi(-z_w)-6k_0z_l(\Delta n_G-\Delta n_L)]\\&+I_5\cos[2\tan^{-1}\xi(z_l)-2\tan^{-1}\xi(-z_l)+6k_0z_l\Delta n_L]\\&+I_6\cos[2\tan^{-1}\xi(z_w)-2\tan^{-1}\xi(-z_l)+3k_0z_l(2\Delta n_L-\Delta n_G)]\\&+I_7\cos[2\tan^{-1}\xi(z_w)-2\tan^{-1}\xi(z_l)-3k_0z_l\Delta n_G]\ ,\end{aligned} \tag{10}$$

where $\Delta n_i=N_i-n_i$ is the dispersion in medium i and $z_l=X\tan\alpha$ represents one half of the liquid thickness at the beam position. Here, α is the wedge angle of the cell window. Equation (10) describes the TH fringe pattern with respect to the translation distance of the liquid cell along the X axis. The intensity parameters I_i ($i=1-7$) of Eq. (10) are related to the transmission factors T_i and the THG susceptibilities (A and R) of air and liquid by

$$\begin{aligned}I_1=&\frac{T_1^2}{[1+\xi^2(-z_w)]^2}+\frac{T_3^2}{[1+\xi^2(z_w)]^2}+\frac{(T_1^2+T_2^2R^2+2T_1T_2R)}{[1+\xi^2(-z_l)]^2}+\frac{(T_3^2+T_2^2R^2+2T_2T_3R)}{[1+\xi^2(z_l)]}\\&+\frac{(2T_0T_1A+A^2T_0^2)}{[1+\xi^2(-z_w)]^2}+\frac{(2T_3T_4A+A^2T_4^2)}{[1+\xi^2(z_w)]^2}\ ;\\I_2=&\frac{(2T_1^2+2T_0T_1A+2T_1T_2R+2T_0T_2AR)}{[1+\xi^2(-z_w)][1+\xi^2(-z_l)]}\ ;\\I_3=&\frac{(2T_1T_3+2T_0T_3A+2T_1T_2R+2T_0T_2AR)}{[1+\xi^2(z_l)][1+\xi^2(-z_w)]}\ ;\\I_4=&\frac{(2T_1T_4A+2T_0T_4A^2+2T_1T_3+2T_0T_3A)}{[1+\xi^2(z_w)][1+\xi^2(-z_w)]}\ ;\\I_5=&\frac{(2T_2^2R^2+2T_1T_3+2T_1T_2R+2T_2T_3R)}{[1+\xi^2(-z_l)][1+\xi^2(z_l)]}\ ;\\I_6=&\frac{(2T_1T_3+2T_1T_4A+2T_2T_3R+2T_2T_4AR)}{[1+\xi^2(-z_l)][1+\xi^2(z_w)]}\ ;\\I_7=&\frac{(2T_2T_3R+2T_2T_4AR+2T_3^2+2T_3T_4A)}{[1+\xi^2(z_l)][1+\xi^2(z_w)]}\ .\end{aligned} \tag{11}$$

We can fit the experimental TH fringe patterns to Eq. (10) to obtain the normalized TH susceptibility of liquid (R) and its dispersion (Δn_L).

IV. EXPERIMENTAL RESULTS

A. Infrared-visible sum-frequency generation from the vapor-liquid interface of CH_3OH-H_2O

The polar orientation of molecules at the vapor-liquid interface of pure methanol has been studied previously by Superfine, Huang, and Shen [15] using IVSFG. Recently, Wolfrum, Graener, and Laubereau [16] applied the same technique to investigate the orientational distribution of methanol molecules at the surface of CH_3OH-H_2O mixtures. In this section, we will concentrate on our experimental results of the polar ordering of methanol molecules at the surface of the binary mixtures of CH_3OH-H_2O in order to directly compare the behavior of the interfacial methanol with that in the bulk of CH_3OH-H_2O.

In Fig. 3 we present four IVSFG spectra of CH_3OH-H_2O with different bulk mole fraction of methanol (c_m).

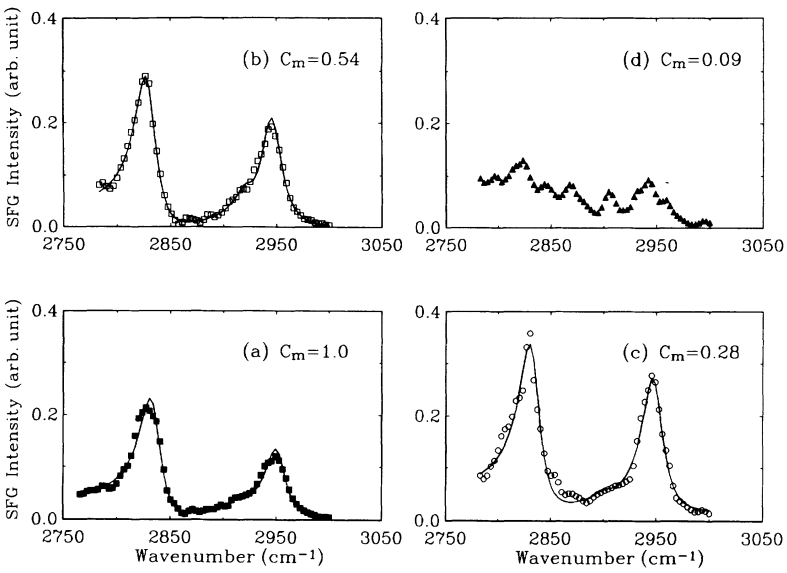

FIG. 3. Measured sum-frequency signal of the liquid-vapor interface in the CH stretching region versus frequency of the input infrared pulse for the methanol-water binary mixture with varying bulk mole fraction (c_m) of methanol molecules. The spectra were taken with the polarization combination of s sum, s visible, and p infrared. The lines are theoretical fits to the absolute square of Eq. (1) to deduce the resonant oscillator strength of the IVSFG susceptibility.

These spectra were taken with the polarization combination of s,s, and p for the sum frequency, visible and infrared beams, respectively. Two major peaks in the C-H stretching region were observed. The peak at 2830 cm^{-1} was assigned to the symmetric stretch of the methyl group (s-CH_3) of methanol molecules, while the other at 2948 cm^{-1} was attributed to the Fermi resonance of the s-CH_3 with overtone of the CH_3 bending mode [15].

It is interesting to note that the SF intensity at the two peaks does not decrease with c_m even when the number density of the bulk methanol molecules in CH_3OH-H_2O has been significantly reduced. These spectra can fit the absolute square of Eq. (1) to deduce the oscillator strength A_q. The resulting A_q at 2830 cm^{-1} as a function of c_m is plotted in Fig. 4 (see the filled squares). According to the theory described above, the SF strength at resonance can fit Eq. (4) with the known surface density of methanol $\bar{N}_s(c_M)$ [17]. The fit (see the solid curve in Fig. 4) yields the following results: $\bar{\chi}_D^{(2)}=\chi_D^{(2)}/\chi_Q^{(2)}=-4.8$ and $G_M(c_m)=6.4c_m^3-13.4c_m^2+8.0c_m$, which indicates that the dipolar contribution is the dominant term in the effective surface SF susceptibility of Eq. (2). The enhancement of the polar ordering (G_M) of the interfacial methanol is plotted in Fig. 5. It is found that G_M achieves a maximum of 1.5 near $c_m \sim 0.2$, then decreases to zero as $c_m \to 0$.

B. Third-harmonic generation from the bulk of CH_3OH-H_2O

In Fig. 6 the THG intensity with different c_m is plotted with the translation distance of the liquid cell along the X axis. At high mole fraction of methanol, the measured THG fringe patterns were found to depend on c_m. However, the fringe patterns appear to be concentration independent when $c_m < 0.3$. We can fit these fringe patterns to Eq. (10) to obtain more quantitative results. In this analysis, the THG susceptibility of air $A \equiv (\chi^{(3)}/\Delta\varepsilon)_{air}/(\chi^{(3)}/\Delta\varepsilon)_{glass}$ was obtained from the comparison between two THG fringe patterns with the empty cell placed in air and in a vacuum chamber. With the known air nonlinearity and index of refraction of the liquid at the pump wavelength, the fit (shown by the solid

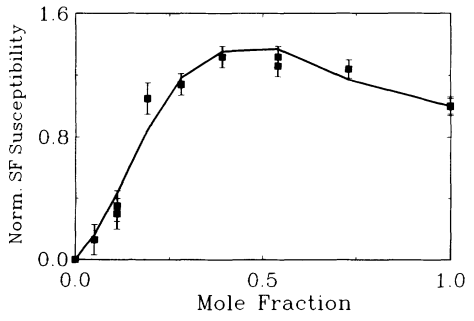

FIG. 4. Measured resonant oscillator strength of the IVSFG susceptibility at 2830 cm^{-1} versus the bulk mole fraction of methanol. The solid curve is theoretical fit to Eq. (4) with the use of the known surface number density of methanol.

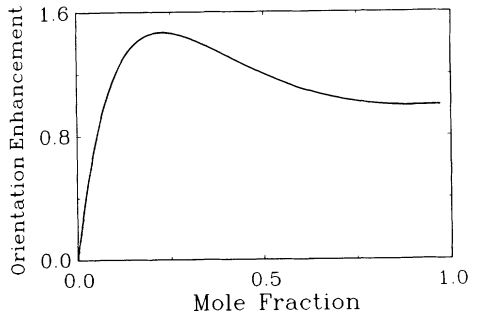

FIG. 5. Enhancement of the polar order of the methanol molecules at the liquid-vapor interface of CH_3OH-H_2O versus the bulk mole fraction of methanol. The curve is deduced from the fit of the measured IVSFG susceptibility at 2830 cm^{-1} to Eq. (4).

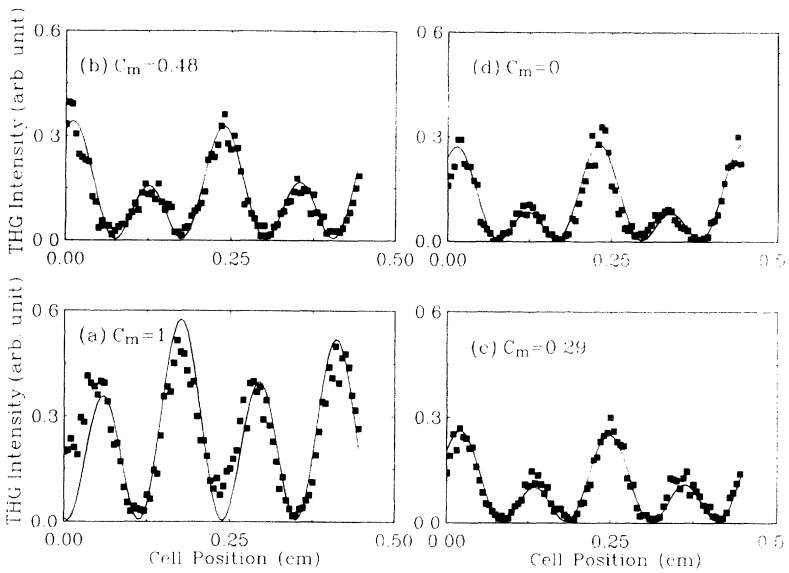

FIG. 6. Third-harmonic-generation Maker fringe patterns obtained from methanol-water binary liquid mixtures with varying bulk mole fraction of methanol (c_m). The solid curves are the theoretical fits to Eq. (10) and the symbols are the data.

curves in Fig. 6) yields the normalized THG susceptibility of the liquid $R \equiv (\chi^{(3)}/\Delta\varepsilon)_L/(\chi^{(3)}/\Delta\varepsilon)_{\text{glass}}$ and its dispersion $\Delta n_L \equiv N_L(3\omega) - n_L(\omega)$.

The resulting liquid nonlinearity $(\chi^{(3)})_L/(\chi^{(3)})_{\text{glass}}$ as a function of c_m is plotted in Fig. 7. The THG susceptibility of the binary liquid mixtures exhibits a complicated dependence on c_m. However, within a narrower range of $0.5 < c_m < 0.9$ a linear behavior was observed. For a sufficiently dilute methanol aqueous solution (i.e., $c_m < 0.3$), $(\chi^{(3)})_L$ appears to be independent of the concentration. But we can find two regions where the TH susceptibility rapidly changes with c_m occur at $0.3 < c_m < 0.5$ and $0.9 < c_m < 1.0$. A simple model will be proposed to illustrate such strange behaviors of CH_3OH-H_2O binary mixtures in Sec. V.

C. Third-harmonic generation from the bulk of CH_3CN-H_2O

Likes methanol molecules, acetonitrile possesses a hydrophobic methyl group. However, it bonds to other molecules through its cyano head group with a single hydrogen bond. It is interesting to know whether such a minor difference can lead to a different liquid structure in CH_3CN-H_2O binary mixtures from that in CH_2CH-H_2O.

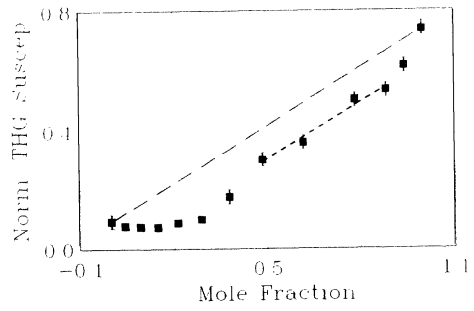

FIG. 7. Measured THG susceptibility of methanol-water mixtures as a function of the bulk mole fraction of methanol. The data of THG susceptibility are normalized with that of fused silica glass.

We have applied THG to study CH_3CN-H_2O with varying mole fraction of acetonitrile (c_a). The results are presented in Fig. 8. The THG fringe patterns appear to be independent of c_a when $c_a < 0.2$. But as $c_a > 0.3$, the concentration dependence of the THG fringe patterns becomes clearly observable. This is more easily seen in the plot of $(\chi^{(3)})_L/(\chi^{(3)})_{\text{glass}}$ as a function of c_a, which is shown in Fig. 9. Within our experimental accuracy as indicated by the error bars, $\chi_L^{(3)}$ of the CH_3CN-H_2O mixtures appears to be a linear function of c_a when $c_a > 0.3$.

V. DISCUSSION

A. Polar ordering of methanol molecules at the vapor-liquid interface of CH_3OH-H_2O

The polar distribution of methanol molecules at the vapor-liquid interface of pure methanol is rather broad. Superfine, Huang, and Shen showed that the symmetric axis of the methyl group of methanol molecules was pointed toward the vapor side with an average tilt angle (θ_0) less than 60° and a full width at half maximum ($\Delta\theta$) larger than 70° [15]. The broad width is consistent with the notion of the highly dynamical nature of the vapor-liquid interface. Computer simulations on the pure methanol predict $\theta_0 \approx 23°$ [18]. Recently, Wolfrum, Graener, and Laubereau with a better signal-to-noise ratio in their IVSFG data further refined these values to be $\theta_0 < 40°$ and $\Delta\theta \approx 70°$ [16]. They also found that the polar order of methanol molecules at the surface of CH_3OH-H_2O increased with a decrease of c_m. At low concentration ($c_m < 0.1$), the angular distribution of the methyl groups was found to be peaked at $\theta_0 \approx 0°$ and $\Delta\theta \approx 16°$ [16].

The fit of the measured $\chi^{(2)}_{s,\text{eff}}(c_m)$ to Eq. (4) allows us to remove the influence of the variation in surface density and the quadrupole contribution from the bulk methanol

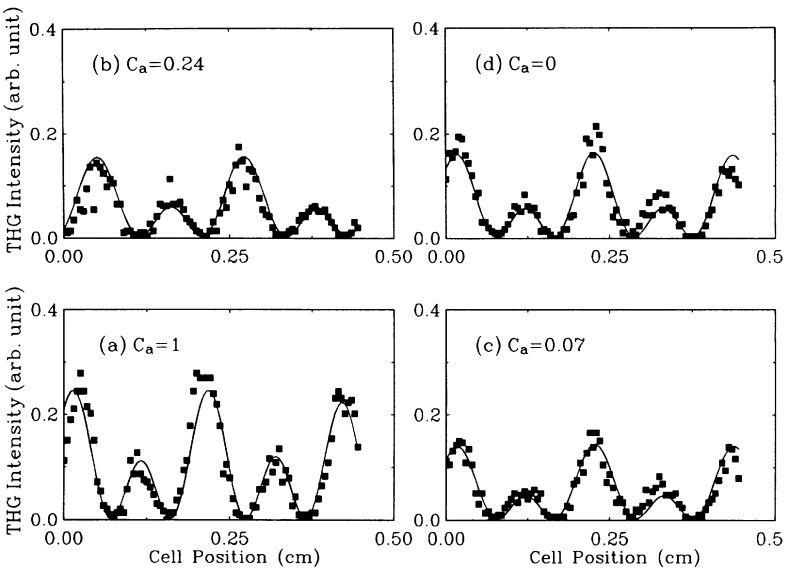

FIG. 8. Third-harmonic-generation Maker fringe patterns obtained from acetonitrile-water binary liquid mixtures with varying bulk mole fraction of acetonitrile (c_a). The solid curves are theoretical fits to Eq. (10) and the symbols are the data.

molecules. The fitting result (shown in Fig. 5) indicates that the enhancement of the polar order of the interfacial methanol increases as the bulk methanol mole fraction is decreased. The enhancement factor achieves a maximum of 1.5 around $c_m \approx 0.2$. A similar conclusion has also been reached by Matsumoto, Takaoka, and Kataoka [19] from a molecular dynamics computer simulation. Notice that $\chi^{(2)}_{s,\text{eff}}(c_m)$ in our IVSFG measurement is proportional to $\langle \sin^2\theta\cos\theta \rangle$ and that $\sin^2\theta\cos\theta$ has a maximum at $\theta \sim 55°$. Assuming a δ function for the polar distribution, $\langle \sin^2\theta\cos\theta \rangle$ is found to decrease with θ if the polar angle is confined to be less than 55°. Considering the hydrophobic nature of the methyl group, the polar angle of the interfacial methanol is unlikely to increase with $(1-c_m)$. Thus the observed enhancement in the polar order of the interfacial methanol molecules cannot simply be attributed to a decrease in polar angle. Instead, if the polar distribution has a full width at half maximum of $\Delta\theta$, an enhancement factor of 1.5 can be yielded with $\Delta\theta$ being decreased from 70° to 0°, while θ_0 is fixed at 27°. It is thus logical to conclude that the reduction in the width of the polar distribution plays the major role in providing the observed enhancement (i.e., $G_M \geq 1$) in our IVSFG measurements. Note that the proton affinity of methanol is about 761 kJ/mole and for water it becomes 697 kJ/mole [20]. When the methanol molecules in the subsurface layer are gradually replaced with water, the stronger hydrogen bond formed between methanol and water molecules may generate a more rigid and directional hydrogen-bonding structure at the vapor-liquid interface of CH_3OH-H_2O, which leads to the decrease in the distribution width of the interfacial methanol molecules with the bulk methanol mole fraction c_m.

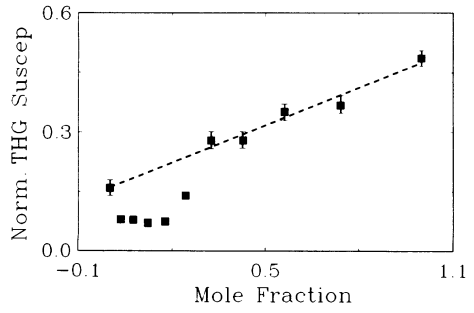

FIG. 9. Measured THG susceptibility of acetonitrile-water mixtures as a function of the bulk mole fraction of acetonitrile. The data of THG susceptibility are normalized with that of fused silica glass.

In Fig. 5, G_M is shown to decrease to zero as $c_m \to 0$. This, however, does not necessarily imply that methanol molecules at the vapor-liquid interface of CH_3OH-H_2O have no polar ordering at low concentration. Instead, we note that G_M simply reflects the orientational averaging of $\sin^2\theta\cos\theta$ over the polar distribution of the interfacial methanol molecules, thus its value can be changed by either varying θ_0 or $\Delta\theta$ as noted above. In fact, our result in Fig. 5, which shows $G_M \sim 0.6$ at $c_m \sim 0.05$, can imply that a distribution of $\theta_0 \sim 0°$ and $\Delta\theta \sim 16°$ appears at $c_m \sim 0.05$. This finding is consistent with the result reported by Wolfrum, Graener, and Laubereau [16].

B. Molecular arrangement in the bulk of CH_3OH-H_2O

In Fig. 7, the THG susceptibility $\chi^{(3)}_T$ of the CH_3OH-H_2O binary liquid mixtures exhibits a nonlinear dependence on methanol mole fraction c_m. $\chi^{(3)}_T$ can be expressed in terms of the THG susceptibility of water ($\chi^{(3)}_W$) and methanol ($\chi^{(3)}_M$) by

$$\chi^{(3)}_T(c_m) = c_m\chi^{(3)}_M + (1-c_m)\chi^{(3)}_W \,. \tag{12}$$

The observed nonlinear behavior of $\chi^{(3)}_T(c_m)$ indicates that either $\chi^{(3)}_M$ or $\chi^{(3)}_W$ must vary with the bulk methanol concentration. In view of the fact that the correlation length of liquid molecules in CH_3OH-H_2O is much shorter than the excitation area of the pump beam, the concentration dependence of $\chi^{(3)}_M$ or $\chi^{(3)}_W$ is most likely caused

by different hydrogen-bonding strength experienced by the liquid molecules as they are mixed.

The binary mixture of methanol and water forms a homogeneous solution because the hydrogen bonding between methanol and water is stronger than that in pure water and neat methanol liquid. For CH_3OH-H_2O at high methanol mole fraction, an insertion of one water molecule into the microstructure of the liquid causes change in the hydrogen-bonding environment of three methanol molecules [see Fig. 10(a)]. This effect leads to the rapid variation in $\chi_T^{(3)}(c_m)$ between $c_m=0.9$ and $=1.0$. At the low concentration limit of methanol, water forms a hydration shell around each methanol molecule [see Fig. 10(b)]. If perturbations on $\chi_W^{(3)}$ by methanol molecules were equally effective as that on methanol molecules by water, we would see a similar dependence of $\chi_T^{(3)}$ on c_m as that observed at the limit of high c_m. On the contrary, $\chi_T^{(3)}$ is nearly constant between $0<c_m<0.3$, which suggests that $\chi_W^{(3)}$ is not sensitive to the chemical-bonding environment.

For the binary liquid mixtures between $0.5<c_m<0.9$, two types of methanol molecules may coexist. The first type of methanol has at least one of its nearest neighbors replaced by water. The THG susceptibility of these methanol molecules will be changed to $\chi_M^{(3)\prime}$

$$\chi_M^{(3)\prime}=\frac{S}{c_\alpha}+\chi_M^{(3)} . \tag{13}$$

Here S denotes the effective perturbation on the THG susceptibility of methanol induced by water. S should be shared among methanol molecules which has a mol fraction of c_α. For the other type of methanol, all its nearest neighbors are not replaced. Thus, $\chi_M^{(3)}$ of this type of methanol will have the same value as that of neat methanol liquid. According to Eq. (12), we can then express $\chi_T^{(3)}$ as

$$\begin{aligned}\chi_T^{(3)}&=[c_m-c_\alpha]\chi_M^{(3)}+c_\alpha\chi_M^{(3)\prime}+(1-c_m)\chi_W^{(3)}\\&=S+c_m\chi_M^{(3)}+(1-c_m)\chi_W^{(3)} .\end{aligned} \tag{14}$$

Thus, a linear dependence of $\chi_T^{(3)}$ on c_m is obtained. Indeed, this is exactly what is observed in Fig. 7 between $0.5<c_m<0.9$. Furthermore, from this experimental result, it suggests that S is negative.

Another region with rapidly changing $\chi_T^{(3)}$ appears between $0.3<c_m<0.5$. Computer simulations suggest that two types of hydrogen bonding [see Fig. 10(b) for the schematic] between water and methanol molecules coexist in a dilute methanol aqueous solution [21]. The observed rapid variation with c_m suggests the onset of an interaction between the methanol molecule and a secondary water molecule. Obviously this interaction sets in when the number of methanol and water in the binary mixtures is equal (i.e., $c_m=0.5$). The interaction should be saturated when the number of water molecules is about two times of methanol ($c_m=\frac{1}{3}$). It is strikingly to observe that $\chi_T^{(3)}$ indeed levels to a constant at $c_m\sim0.3$. The hydration shell of a methanol may be complete below this concentration. Soper and Finney recently conducted a neutron diffraction study of the CH_3OH-H_2O mixture with a methanol mole fraction of 0.1 [22]. They confirmed the existence of a definite hydration shell of water molecules at a distance of ~3.7 Å from the carbon atom in the methanol molecule.

We are now at the stage to explain why the THG susceptibility of the CH_3OH-H_2O mixtures is smaller than that predicted by Eq. (12). First, we note that electron correlation is indispensable for an accurate description of the NLO response of molecules [23–25]. Quantum chemical calculation without including electron correlation often underestimates the nonlinear polarizability of molecules. Note that hydrogen bonding may partially freeze electron movement and thus reduces electron correlation. Indeed according to a computer simulation study reported by Ikata [26], including electron correlation leads to a reduction in the hydrogen-bonding strength of $CH_3OH\ldots H_2O$. It appears to be that the effect of electron correlation cancels off the effect induced by hydrogen bonding. Based on the above discussion, a smaller value of the NLO susceptibility can be yielded from a solution with stronger solute-solvent hydrogen bonding. This is experimentally supported from our result that S parameter in Eq. (13) is negative for CH_3OH-H_2O compared with the result predicted from a model of independent-liquid mixtures.

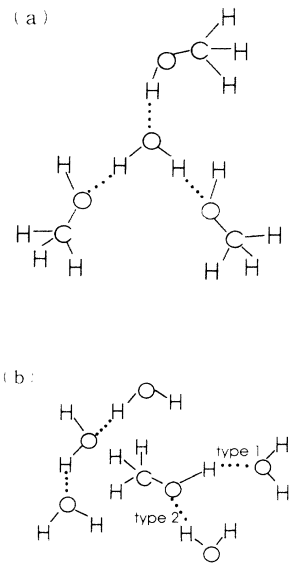

FIG. 10. Schematic diagram shows the molecular arrangement in the methanol-water mixture at (a) high c_m; and (b) low c_m. The dotted lines denote the hydrogen bonding. The tetrahedral bonding geometry around the oxygen atom in a water molecule has been simplified in this schematic.

C. Molecular structure in the bulk of CH_3CN-H_2O binary mixtures

In the CH_3CN-H_2O binary mixtures, an abrupt change in the THG susceptibility was observed to appear at an acetonitrile mol fraction of 0.3. When $c_a>0.3$, $\chi_T^{(3)}(c_a)$ can be described very well with Eq. (12) (see the dashed line in Fig. 9) by assuming that $\chi_A^{(3)}$ and $\chi_W^{(3)}$ are constant.

Theoretical studies suggest the existence of microheterogeneity in these binary liquid mixtures [27]. The tendency of preference for neighbors of the same kind extends over several concentric shells around a given molecule. If such a microstructure indeed happens, then $\chi_W^{(3)}$ and $\chi_A^{(3)}$ in the mixtures should keep at the values of neat liquids. Therefore $\chi_T^{(3)}$ of the binary mixtures will follow Eq. (12), which explains the observed linear behavior of $\chi_T^{(3)}(c_a)$ for $c_a > 0.3$.

The structure of the CH_3CN-H_2O binary mixtures has been explored by Marcus and Migron [27] by use of thermodynamic data and the inverse Kirkwood-Buff integral method. They also propose an interesting picture for the CH_3CN-H_2O mixtures that acetonitrile molecules first enter in the water structure at low acetonitrile concentration. The limit of c_a beyond which the acetonitrile cannot any longer be accommodated within the cavities of the structure of water lies in the range $0.10 \leq c_a \leq 0.33$. Beyond this limit the microheterogeneity sets in. Note that although acetonitrile has a larger proton affinity of 787 kJ/mole [20], it can only provide a single hydrogen bonding for each molecule. At low c_a a phase of homogeneous solution indeed can reduce Gibbs free energy in view of the stronger hydrogen bonding of $CH_3CN\ldots H_2O$. This is also supported by the smaller $\chi_T^{(3)}$ than that of independent-liquid mixtures between $0 < c_a < 0.3$. But at higher c_a (e.g., > 0.3) a structure of microheterogeneity can have a smaller Gibbs free energy by maximizing the number of hydrogen bonds in the liquid.

D. Polar distribution of acetonitrile molecules at the vapor-liquid interface of CH_3CN-H_2O

An IVSFG study of the structure of the interfacial acetonitrile molecules at the surface of CH_3CN-H_2O has been reported by Zhang *et al.* [7]. They discovered that the resonant frequency of the CN stretching mode experiences a sudden redshift when the bulk acetonitrile concentration c_a was increased above 0.07 [7]. Together with the frequency shift, the averaged polar angle of the interfacial acetonitrile molecules also exhibits an abrupt change from 40° to 70°, when c_a is increased through this critical point. The polar angle of CH_3CN was found to decrease with an increase in the interfacial water molecules. This behavior is similar to what has been observed on CH_3OH at the surface of CH_3OH-H_2O mixtures. This finding supports the notion that the hydrophobicity of the methyl group in methanol and acetonitrile plays an important role in determining their polar orientation at the liquid surface.

The abrupt change in the resonant frequency and polar orientation of the interfacial CH_3CN was attributed by Zhang *et al.* to the disappearance of the hydrogen bonding between the interfacial H_2O and CH_3CN when $c_a > 0.07$, which implies the existence of a surface phase separation above this concentration.

Here some factors may be considered for elucidating why the mole fraction of acetonitrile at the onset of surface phase separation is smaller than that appearing inside the liquid. First, the asymmetric interaction, which leads to better oriented interfacial acetonitrile molecules, may play a role in reducing the critical concentration of phase separation. The second, it is noted that acetonitrile can act as surfactant molecules of CH_3CN-H_2O binary mixtures owing to the hyrophobic nature of its methyl group. Thus, the actual surface mole fraction of acetonitrile can be higher than that in the liquid. The driving energetic mechanism of the phase separation in CH_3CN-H_2O as discussed in the above section should be equally applicable for the surface structural change.

VI. CONCLUSIONS

Two nonlinear optical techniques have been applied to study two important binary liquid mixtures of hydrogen bonded liquids. For CH_3OH-H_2O, the measured THG susceptibility with varying methanol mole fraction was found to reflect the detailed microscopic structure of the mixtures. The structural information of a liquid surface can be yielded from an infrared-visible sum-frequency generation (IVSFG) study. With this technique the polar distribution of the methanol molecules at the surface of CH_3OH-H_2O was found to be enhanced by the interfacial water molecules. For CH_3CN-H_2O mixtures, our THG measurements support the existence of microheterogeneity in the liquid mixtures with acetonitrile mole fractions higher than 0.3. This critical concentration for the bulk phase separation is larger than that appearing at surface. The different behaviors of CH_3OH-H_2O and CH_3CH-H_2O mixtures are surprising in view that acetonitrile and methanol are similar in their molecular structures. Our results indicate that by combining THG and IVSFG the detailed molecular structure at the surface and in the bulk of a liquid can be probed without perturbing the equilibrium of the liquid.

ACKNOWLEDGMENT

This work was supported by a grant from the National Science Council of R.O.C. under No. NSC82-0208-M-009-037. The author (J.Y.H.) thanks Professor Y. R. Shen for his stimulating discussion and critical reading of this manuscript.

[1] See, for example, *Hydrogen Bonded Solvent Systems,* edited by A. K. Covington and P. Jones (Taylor and Francis, London, 1968); J. S. Rowlinson and F. L. Swinton, *Liquids and Liquid Mixtures,* 3rd. ed. (Butterworths, London, 1982).

[2] R. Pethig, Annu. Rev. Phys. Chem. **43**, 177 (1992).

[3] W. Kauzmann, Adv. Protein Chem. **14**, 1 (1959).

[4] H. Bertagnolli and M. D. Zeidler, Mol. Phys. **35**, 177 (1978), and references therein.

[5] Y. R. Shen, Nature (London) **337**, 519 (1989), and references therein.

[6] W. K. Burns and N. Bloembergen, Phys. Rev. B **4**, 3437 (1971); F. Kajzar and J. Messier, Phys. Rev. A **32**, 2352 (1985); J. E. Sipe, D. J. Moss, and H. M. van Driel, Phys.

Rev. B **35**, 1129 (1987); G. Lupke and G. Marowsky, Appl. Phys. B **53**, 71 (1991); D. M. Burland, C. A. Walsh, F. Kajzar, and C. Sentein, J. Opt. Soc. Am. B **8**, 2269 (1991).

[7] D. Zhang, J. H. Gutow, Eisenthal, and T. F. Heinz, J. Chem. Phys. **98**, 5099 (1993).

[8] P. Guyot-Sionnest, J. H. Hunt, and Y. R. Shen, Phys. Rev. Lett. **59**, 1597 (1987); Chem. Phys. Lett. **133**, 189 (1987); **1**, 144 (1988).

[9] F. Kajzar and J. Messier, Rev. Sci. Instrum. **58**, 2081 (1987).

[10] P. Guyot-Sionnest, W. Chen, and Y. R. Shen, Phys. Rev. B **33**, 8254 (1986); P. Guyot-Sionnest and Y. R. Shen, *ibid.* **35**, 4420 (1987); **38**, 7985 (1989), and references therein.

[11] J. Y. Huang and Y. R. Shen, *Sum-Frequency as a Surface probe,* edited by H. L. Dai and W. Ho, in Laser Spectroscopy and Photochemistry on Metal Surfaces (Academic Press, San Diego, 1993), Chap. 1.

[12] J. F. Ward and G. H. New, Phys. Rev. **185**, 57 (1969).

[13] H. Puell, K. Spanner, W. Falkenstein, W. Kaiser, and C. R. Vidal, Phys. Rev. A **14**, 2240 (1976).

[14] G. C. Bjorklund, IEEE J. Quantum Electron. **QE-11**, 287 (1975).

[15] R. Superfine, J. Y. Huang, and Y. R. Shen, Phys. Rev. Lett. **66**, 1066 (1991).

[16] K. Wolfrum, H. Graener, and A. Laubereau, Chem. Phys. Lett. **213**, 41 (1993).

[17] J. J. Kipling, J. Colloid Sci. **18**, 502 (1963).

[18] M. Matsumoto and Y. Kataoka, J. Chem. Phys. **90**, 2398 (1988).

[19] M. Matsumoto, Y. Takaoka, and Y. Kataoka, J. Chem. Phys. **98**, 1464 (1993).

[20] B. J. Smith and L. Radom, J. Am. Chem. Soc. **115**, 4885 (1993).

[21] S. Okazaki, K. Nakanishi, and H. Touhara, J. Chem. Phys. **78**, 454 (1983).

[22] A. K. Soper and J. L. Finney, Phys. Rev. Lett. **71**, 4346 (1993).

[23] G. D. Purvis, III and R. J. Bartlett, Phys. Rev. A **23**, 1594 (1981).

[24] F. Sim, S. Chin, M. Dupuis, and J. E. Rice, J. Phys. Chem. **97**, 1158 (1993).

[25] A. Willetts and J. E. Rice, J. Chem. Phys. **99**, 426 (1993).

[26] S. Ikata, J. Computational Chem. **5**, 374 (1984).

[27] Y. Marcus and Y. Migron, J. Phys. Chem. **95**, 400 (1991).